Eur. Phys. J. A **3**, 325–333 (1998)

THE EUROPEAN PHYSICAL JOURNAL A

Formation and deexcitation of the composite nucleus in the Ni + Al reaction at 28 A·MeV

L. Lebreton[1], D. Benchekroun[1], E. Bisquer[1], B. Chambon[1], B. Cheynis[1], A. Demeyer[1], D. Doré[3], D. Drain[1], E. Gerlic[1], D. C. R. Guinet[1], P. Lautesse[1], C. Pastor[1], M. Stern[1], L. Vagneron[1], C. Vincent-Donnet[1], A. Chabane[2], A.J. Cole[2], P. Désesquelles[2], A. Giorni[2], D. Heuer[2], A. Lleres[2], J.B. Viano[2]

[1] Institut de Physique Nucléaire de Lyon (CNRS-IN2P3 et Université Claude Bernard), 43 Bd du 11 novembre 1918, F-69622 Villeurbanne Cedex, France.
[2] Institut des Sciences Nucléaires de Grenoble (CNRS-IN2P3 et Université Joseph Fourier), 53 Avenue des Martyrs, F-38026 Grenoble Cedex, France.
[3] Centre d'Etudes Nucléaire de Saclay (CEA DAPNIA/SphN), 91191 Gif sur Yvette Cedex, France

Received: 11 February 1998 / Revised version: 1 August 1998
Communicated by V. Metag

Abstract. The formation and the deexcitation of the composite nucleus formed during the Ni + Al reaction at 28 A·MeV has been studied with the 4π multidetector AMPHORA. A rigourous selection of the experimental data is described in order to extract a central collision sample. Then different models are compared to the data. The incomplete fusion process is in agreement with the data. The azimuthal angle correlations of He-Li and Li-Li pairs have been used to discriminate sequential or instantaneous emission. The sequential deexcitation is more consistent with all the data. The different analyses allow to describe all the characteristics of the compound nucleus and finally a fusion cross section of 300 ± 100 *mbarn* has been measured.

PACS. 25.70 Pq Multifragment emission and correlations

1 Introduction

Heavy ion studies have taken a new interest since 4π detectors were designed. Indeed the accuracy of the measurement has been improved and allows a better understanding of the basic mechanisms in nuclear collisions. In the experiment described hereafter, we are interested in the deexcitation process of a hot source created by the reaction between the nickel projectile and the aluminium target for an incident energy of 28 A·MeV. We will focus more specifically on light charged particles and Intermediate Mass Fragment emission (IMF is defined as a fragment with charge Z $\geq$ 3 and Z $\leq$ Z_{proj}). The points we would like to address are the following:
– do we form a "single source"? If so, how to select the single source data to determine the characteristics of this source?
– concerning the deexcitation of this source, do we observe a sequential or instantaneous IMF emission?
Obviously these points are related to the observation of the composite system multifragmentation in the central collisions. The incident energy of this experiment is in the transition region between:
– the low energies ($E_{inc} \leq$ 15-20 A·MeV) where the reaction mechanisms are governed essentially by the long range part of the nuclear force, hence by mean field [1]. Complete or incomplete fusion is observed for central collisions and the compound nucleus deexcitation is mainly composed by light charged particles evaporation. Binary dissipative collisions are observed for peripheral collisions and the deexcitation process of both excited quasi-target and quasi-projectile is identical to the compound nucleus one.

– the high energies ($E_{inc} \geq$ 100 A·MeV) where the reaction mechanisms are governed by nucleon-nucleon interaction leading to the so called participant-spectator picture [2].

In-between the situation is more complicated, since experimentally the IMF production appears to be relevant of the low energy mechanisms evolution or/and of the apparition of new ones. This region creates a large interest since the question of the phase transition has appeared recently [3]. The composite system multifragmentation has been observed for both light systems [4,5] like the Ca + Ca 35 A·MeV reaction [6] and heavy systems [7,8] like the Xe + Sn 50 A·MeV reaction [9]. The present paper describes the results of the Ni + Al reaction at 28 A·MeV which is in the low part of the transition region where the multifragmentation process is expected to appear.

Section two will present the experimental set-up, section three will describe the event selection, section four

will focus on the data analysis and then section five will discuss the results.

2 Experimental procedure and data reduction

The experiment was performed at the SARA facility, in Grenoble, using the AMPHORA multidetection array. This experiment involved a 28 A·MeV ^{58}Ni beam on a ^{27}Al target. AMPHORA is an azimuthally symmetric multidetector made of 140 charged particle detectors covering 82% of 4π (AMPHORA has been described in detail in previous work [10]). It is divided into a forward wall section which contains 48 CsI (2°- 16°) and a 92 CsI backward ball (16°- 165°). Thin plastic scintillators (100 and 200 μm) set in the front of the CsI detectors (up to 38°) allow identification of charge up to Z = 30 within ±1 charge unit. For CsI detectors at polar angles larger than 38°, the identification was limited to charge Z ≤ 3. A multiplicity threshold of two was imposed during the experiment with the aim of rejecting the most peripheral collisions.

The energy calibration was carried out in a separate experiment with the same beam and target. During this calibration experiment, silicon tri-telescopes (50, 150 and 500 μm) were used together with a 3 cm CsI(Tl) crystal which measured energy spectra at each polar angle covered by the AMPHORA detectors. For each polar angle ring of AMPHORA one detector was selected as a reference and the gains for other detectors in the same ring were adjusted to reproduce the reference detector spectrum. It was then sufficient to calibrate the reference detector using the energy spectra measured in the calibration run at the corresponding polar angles.

For detectors equipped with plastic scintillators it has been found (by extending the work of [12] and [13]) that the energy of an ion with charge Z can be written as:

$$\mathrm{E_r} = \mathrm{A} * \mathrm{L} + \mathrm{B} * \ln(1 + \mathrm{C} * \mathrm{L}) \qquad (1)$$

where, for each Z, $\mathrm{E_r}$ is the energy deposited in the CsI crystal, L is the light output of the CsI crystal minus the light corresponding to the energy loss in the plastic scintillator and:

$$A = (\alpha_1 * Z + \alpha_2)Z$$
$$B = (\beta_1 * Z + \beta_2)Z$$
$$C = (\gamma_1 * Z + \gamma_2)Z^2$$

where $\alpha_\mathrm{i}, \beta_\mathrm{i}, \gamma_\mathrm{i}$ are constants determined for each reference detector.

Calibration for charge one was eased by the observation of punch through energies in the CsI detectors.

The energy thresholds for the CsI crystals are 4 MeV for protons, 7 MeV for alpha particles and 10 MeV for lithium. For the plastic foils of 200 μm thickness, they are 4 MeV for protons, 14 MeV for alphas, and 6-10 A.MeV for ions of charges Z = 5-15.

In order to prevent particle contamination from other beam bursts, we have checked particle time origin. For all detectors equipped with a plastic foil, a time signal was measured using a start given by the cyclotron radio frequency. The effective time gate of the data acquisition included two beam bursts. During off-line analysis we retained only events coming from the same burst. More precisely, if an event contains at least one particle which does not belong to this burst the full event is rejected. We have checked that the rejection rate is negligible.

3 Event selection

Due to the AMPHORA design and to the reverse kinematics of this reaction, it has been possible to detect quasi-complete events, involving at least 80% of the total charge detected ($33 \leq \mathrm{Z_{total}} \leq 41$). Figure 1 shows for each event the total parallel momentum versus the total charge for experimental data. It can be noticed that the requirement of quasi-complete detection of the total charge implies the detection of at least 60% of the incident parallel momentum (13 GeV/c).

The first goal is to select central collisions, the fragments produced in peripheral collisions for this system, are mainly emitted along the beam axis (quasi-projectile fragments) and then go through the forward hole or are stopped in the plastic detectors (quasi-target fragments) due to energy thresholds. Consequently by requiring quasi-complete measurement of the total charge, we detect mostly central events.

For a quantitative illustration of this correlation between the total detected charge and the centrality of the reaction we have performed numerical simulations with the DBS code ("Diffusion Binaire Séquentielle") [14], which describes the full range of impact parameters from central collisions (b ≃ 0 fm) to the most peripheral

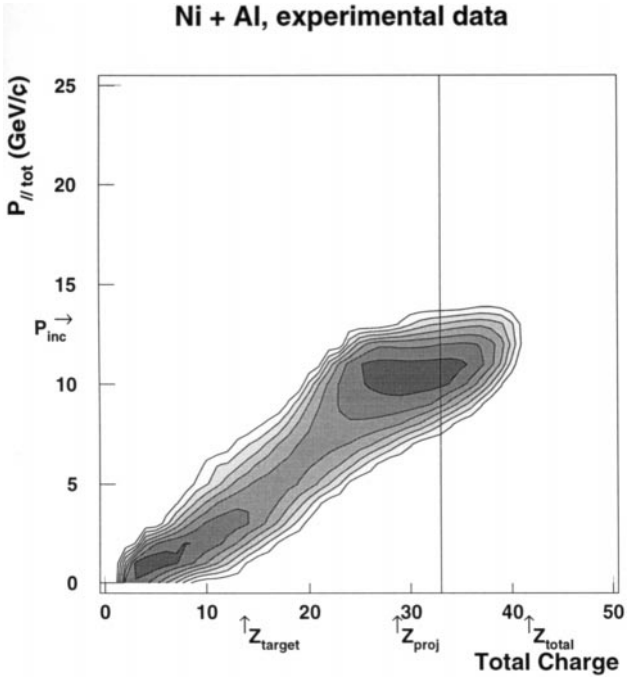

Fig. 1. Total parallel momentum versus the total charge detected with AMPHORA. The line represents 80% of total charge Z_{total}

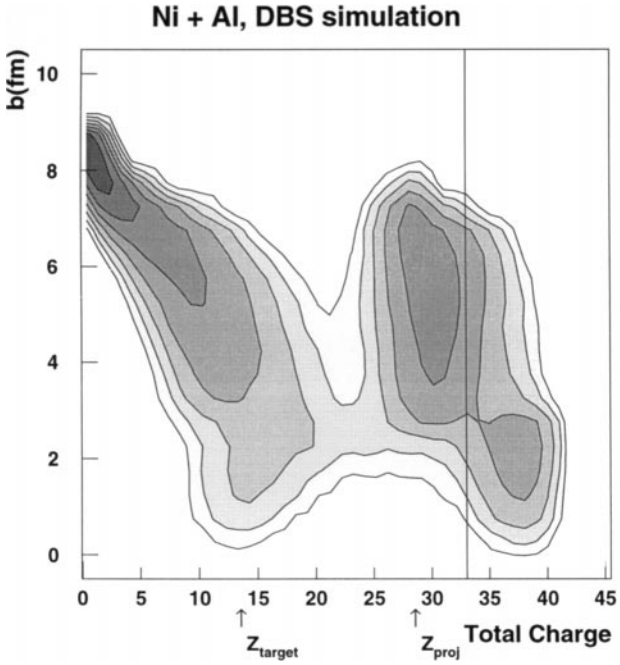

Fig. 2. Correlations between the total charge detected with AMPHORA and impact parameter. Events are generated by the DBS code as described in the text and filtered.The line corresponds to 80% of total charge Z_{total}

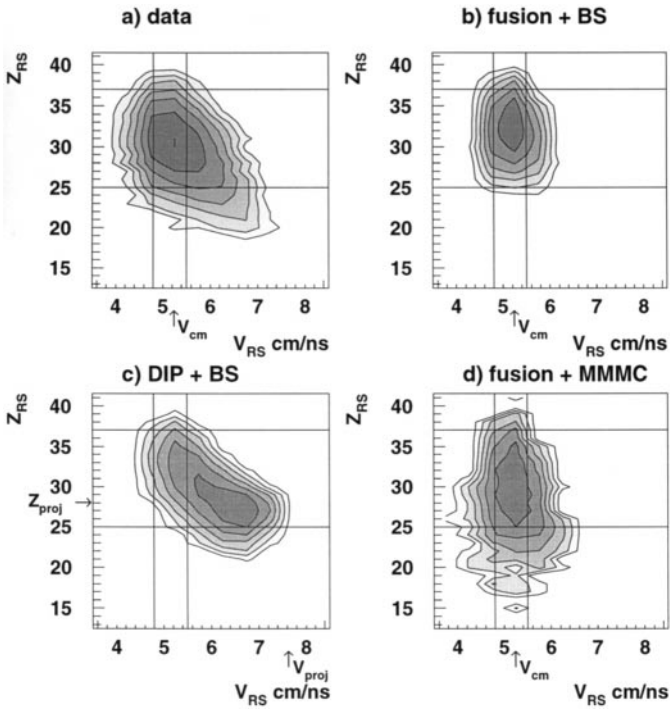

Fig. 3. a–d Source Reconstitution Method. These plots represent the charge of the reconstituted source versus the velocity of this source. **a** experimental data, **b** simulation of fusion followed by sequential deexcitation (DBS code), **c** simulation of DIP followed by sequential deexcitation (DBS code), **d** fusion and MMMC. All events (experimental events and simulated ones) are quasi-complete. V_{cm} is the center of mass velocity, V_{proj}, Z_{proj} are respectively the projectile velocity and charge

collisions (b = 8.7 fm). The results of these calculations are afterwards filtered by the SIR code ("SImulateur de Réponse" [15]) in order to simulate the detector response.

– The DBS code simulates the nuclear collision dynamics taking into account preequilibrium emission and the deexcitation following the reaction. The calculation is performed for a given impact parameter generated by randomly drawing from a triangular distribution. The fusion and the Deep Inelastic Process (DIP) probabilities are estimated by solving the classical dynamical equations [17]. Trajectory equations take into account Coulomb, nuclear conservative and nuclear friction dissipative forces. The entrance channel leads to either the formation of an excited composite nucleus or a binary process resulting in a quasi-target and a quasi-projectile both excited. Then the GEMINI code [18] is used to describe sequential decay for the excited composite nucleus or for the excited quasi-target and quasi-projectile.

In Fig. 2 we show the correlation between the impact parameter and the total detected charge for simulated events. Most of the events detected with the largest total charge corresponding to the most central collisions are related to the lowest impact parameters. In the figure three parts can be observed. For total charge lower than 23, the events are poorly detected. This corresponds to binary events where one or several fragments are missed and the lack of information gives difficulties to analyze these data. For total charge greater than 23, two bumps are visible, the first one covering impact parameters from 0 to 3 fm where the fusion process is expected, the second one from 3 to 8 fm where the deep inelastic process is involved. Therefore the first event selection, in order to isolate the most central collisions, is the selection of quasi-complete events ($\geq$ 80 % of Z_{Total}, see corresponding line in the figure). Nevertheless by requiring quasi-complete detection of the total charge, the DBS code calculations indicate that 56% of simulated events originate from the deep inelastic process (DIP). This contribution comes mainly from the large impact parameters (b $\geq$ 3 fm) as it can be seen in Fig. 2.

To reduce the DIP proportion we have employed the reconstitution source method [19]. The selected sample with the first criteria are analyzed within the following procedure.

This method is based on the heaviest fragment detected in each event. In a first iteration the heaviest fragment determines the source velocity. In this source frame three velocity spheres are built. The first for Z = 1, the second for Z = 2, the last for Z $\geq$ 3. The radii are respectively equal to $0.6v_{beam}$, $0.5v_{beam}$ and $0.4v_{beam}$. All particles which are in these spheres are supposed to be emitted by the source. In Fig. 3 we report this reconstitution process for the experimental data (Fig. 3a) for simulation of fusion followed by sequential deexcitation (DBS code, Fig. 3b) and for deep inelastic process followed by sequential deexcitation (DBS code, Fig. 3c) and of fusion

followed by an instantaneous multifragmentation (MMMC code, Multifragmentation Microcanonical Monte Carlo developped by D.H.E. Gross and collaborators [20]) (Fig. 3 *d*). We will discuss this last figure later in the text. First, the DBS fusion events Fig. 3b are correctly reconstructed $< Z_{RS} > = 32$ and the $< V_{RS} > \simeq V_{cm}$. The slight difference on the $< Z >$ observed in Fig. 2 comes from the reconstruction method which does not keep the large velocity for the light particles, but the difference is small. Second, the DBS DIP events are also well reproduced and the average velocity is smaller than the projectile one since the first selection cuts the most peripheral events.

So to separate fusion events from the DIP ones in the selected data, a second criterion based on the reconstructed source coming from data is used.

This new event selection consists of laying down conditions about the velocity and the charge of the reconstituted source. These selections are represented by four lines upon each plot of Fig. 3 and are:

$$25 \leq \mathrm{Z_{RS}} \leq 37$$
$$4.8 \leq \mathrm{V_{RS}} \leq 5.5\,\mathrm{cm/ns}$$

where $\mathrm{Z_{RS}}$ is the reconstructed source charge and $\mathrm{V_{RS}}$ the reconstructed source velocity.

The DBS code indicates that, after these selections, in the simulated data the fusion events are dominant (80%) but a small component of binary inelastic events are present. These DIP events result from the smallest impact parameters for this process as it can be seen in Fig. 2. Finally the two criteria have been used to prepare our sample data for the analysis.

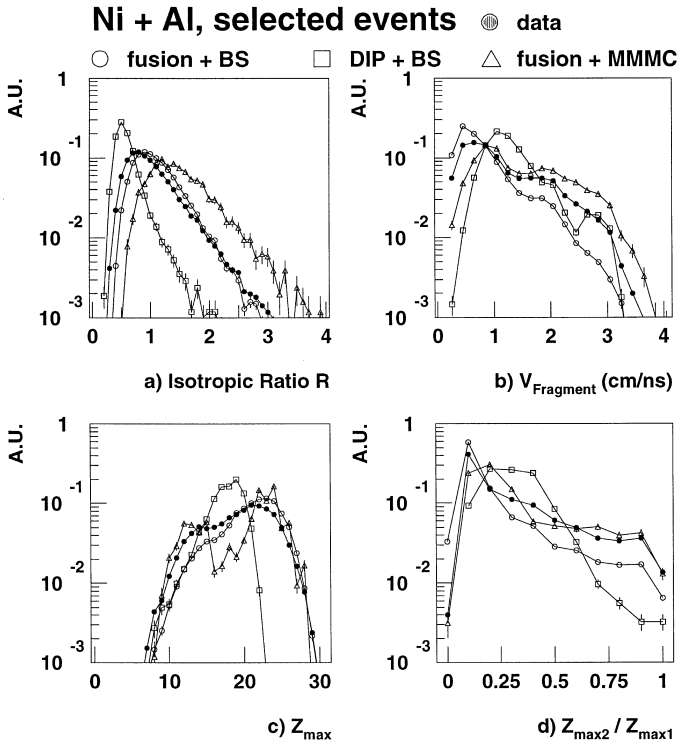

Fig. 4. Comparisons between data and simulations, fusion + BS (open circles), fusion + MMMC (open triangles), DIP + BS (open squares) and experimental data (black circles) for the most discriminating variables: **a** isotropic ratio, **b** fragment velocity, **c** charge distribution of the heaviest fragment, **d** charge ratio between the two heaviest fragments

4 Data analysis

In this section comparisons between data and different scenarios will be done. To realize these comparisons, four experimental variables have been chosen, related, either to dynamics like the isotropic ratio or the center of mass velocity, either to static properties of the reaction like the charge of the biggest fragment or the ratio between the charge of the two biggest fragments. Then the azimuthal correlation analysis is described and used to estimate the angular momentum of the emitter and the time delay between the emision of two charged particles.

The main experimental characteristics of the selected events (the selected sample represents 13 % of the raw data) are presented in Fig. 3a, 4 *a b c d*. Let us complete these figures with some other features:

- the mean charged particle multiplicity is 10
- the mean IMF multiplicity is two, one big fragment $Z_{1max} \simeq 20$ and the second one $Z_{2max} \simeq 5$

4.1 Comparisons with numerical calculation - Deexcitation modes of the excited source

In order to confirm or invalidate the DBS code predictions (80% of supposed fusion process present in our sample of selected events) and to understand the source deexcitation, the experimental data have been compared with 3 numerical simulations (involving the same selections). The first one simulates a fusion source which deexcites by sequential emission of light particles and IMF (Fig. 3b), the second one is a simulation of a very deep inelastic process in which the quasi-projectile and the quasi-target deexcite by sequential decay (Fig. 3c), the last one is fusion followed by simultaneous multifragmentation simulation (Fig. 3d). For the latter code the input data are characteristics of the compound nucleus (preequilibrium emission is not taken into account). A first overlook indicates that the fusion + BS or fusion + MMMC simulations have a general agreement with the data while the DIP + BS one does not reproduce correctly the data. These figures lead to the conclusion that the fusion process seems to be dominant whatever the deexcitation process, but as shown by the simulation, a contamination of DIP is observed since a small part of this process is included in our selection.

Figure 4 presents comparisons between experimental and simulated data for the most discriminating variables. The isotropic ratio $\mathrm{R} = (2/\pi) * \mathrm{P_{\perp}^{tot}}/\mathrm{P_{\parallel}^{tot}}$ is shown in Fig. 4a, where $\mathrm{P_{\perp}^{tot}}$ is the total transverse momentum of the event and $\mathrm{P_{\parallel}^{tot}}$ is the total parallel momentum. The experimental data (black circles) are in better agreement with the fusion + sequential deexcitation process (open

circles) comparred to the DIP + sequential deexcitation process (open squares). This result confirms that fusion events are a major part of the selected events as already shown in Fig. 3.

The same conclusion is obtained from the fragment velocity distribution in Fig. 4b, this plot takes into account only fragments with a charge greater than 6 and the velocity is calculated in the system rest frame. It is also true for the Z_{max} distribution (maximum charge in the event) in Fig. 4c and for the ratio between the charge of the heaviest fragment and charge of the second heaviest fragment in Fig. 4d. Considering these variables we conclude that the behaviour of the experimental data is reproduced by a fusion process in the first stage of the reaction followed by sequential decay rather than a deep inelastic process. However the multifragmentation process cannot be excluded, if one observes a rough agreement with the selected data in Fig. 4bcd, for Fig. 4a the fusion + sequential decay gives a better data reproduction.

The azimuthal correlation analysis occurs several places [23] to get some additional informations on the angular momentum of the emitter and on the time delay between the fragment emission. The fits between the DBS results and experimental data allow us to use the parameters of the DBS source as inputs in the MODGAN code for the azimuthal correlations analysis. These parameters are the outputs fixed by DBS:

$$\begin{aligned} &< E^*_{CN} >= 414\text{MeV} \\ &< \varepsilon^*_{C.N.} > \simeq 5\text{A} \cdot \text{MeV} \\ &< Z_{CN} >= 38 \\ &< A_{CN} >= 80 \\ &< J_{CN} >= 37\hbar \end{aligned}$$

where E^*_{CN}, Z_{CN}, A_{CN}, J_{CN} are respectively the excitation energy, the charge number, the mass number and the angular momentum of the compound nucleus. It is important to note that this angular momentum is not a free parameter, it is determined by the DBS calculation and this parameter is not used as input for MODGAN. On the contrary, we check the average angular momentum given by MODGAN with this one.

4.2 Azimuthal correlation analysis

To further analyze the features of the source decay and to deduce the angular momentum of the emitter we have used the azimuthal correlations analysis doing comparisons with the MODGAN code [21].

4.2.1 The MODGAN code

The particle emission is described in terms of sequential emission from an equilibrated rotating source. The emission direction is determined by a statistical process, the emission probability $d\Gamma_{E,\boldsymbol{J},f}$ of a fragment f with energy E from the source with angular momentum $\boldsymbol{J}$ is written:

$$d\Gamma_{E,\boldsymbol{J},f} \propto e^{\beta_2 \sin^2(\Psi_{\boldsymbol{J},f})} \quad (2)$$

where $\Psi_{\boldsymbol{J},f}$ is the angle between the emission direction of the fragment f and the angular momentum $\boldsymbol{J}$ axis of the source. β_2 is called the anisotropy ratio:

$$\beta_2 = \frac{\hbar^2(J+1/2)^2}{2I_d T}\left(\frac{\mu R^2}{I_d + \mu R^2}\right) \quad (3)$$

where:

- I_d is the moment of inertia of the compound nucleus
- R the position of the center of mass (particle + residual system)
- μ the mass of the reduced system
- T the emitter temperature

In the MODGAN code lifetime effects are taken into account by solving the classical trajectory equations with the three body Coulomb interaction.

4.2.2 Construction of azimuthal correlations and characteristics

The azimuthal correlation is constructed from the distribution of relative angles between two detected particles (belonging to the same event). To suppress the effect of detector geometry and detection efficiency we use only the four first rings of AMPHORA (for polar angles 20°, 31°, 47°, 67°). These rings are identical: 15 detectors with the same response.

To construct the azimuthal correlation between two particles $X(\theta_X, \phi_X)$, $Y(\theta_Y, \phi_Y)$ we isolate events for which we have detected at least one particle X at the θ_X polar angle, and one particle Y at the θ_Y polar angle, then we calculate:

$$\Delta\phi = |\phi_Y - \phi_X|$$

The distribution is normalized such that the mean value is one.

To check the MODGAN code results, we have used the angular momentum of the fusion events coming from the DBS simulation. Figure 5 presents the azimuthal correlation distribution for the DBS fusion events and the MODGAN simulation for angular momenta of 40 $\hbar$ and 60 $\hbar$ for the He-He pairs. The agreement is good for 40 $\hbar$ which is compatible with the DBS value of 37 $\hbar$ as mentionned above. We can conclude that the MODGAN code is well calibrated.

In order to observe the angular momentum and time delay emission effects we have plotted the azimuthal correlations between lithium and helium pairs generated with the MODGAN code. In a previous paper [22] both effects for the angular momemtum value and for the time delay between the emission of two particles have been shown. Recall that the anisotropy is larger when the emitted particle mass increases and that a suppression at small angular correlations is observed due to Coulomb repulsion.

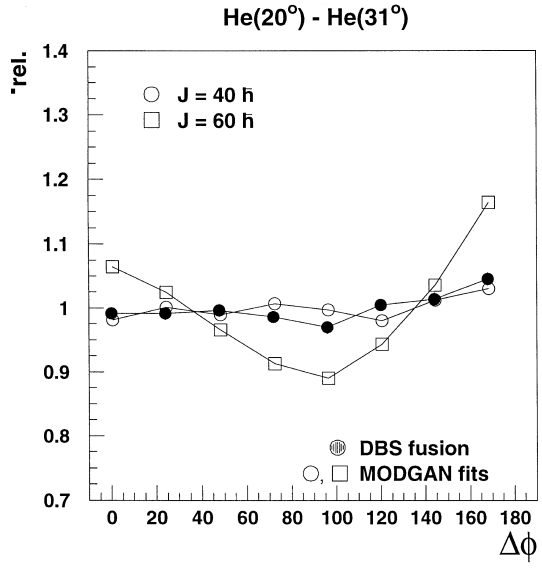

Fig. 5. Adjustment of azimuthal correlation distribution for the DBS fusion events ($< J > \simeq 37\hbar$) by the MODGAN code

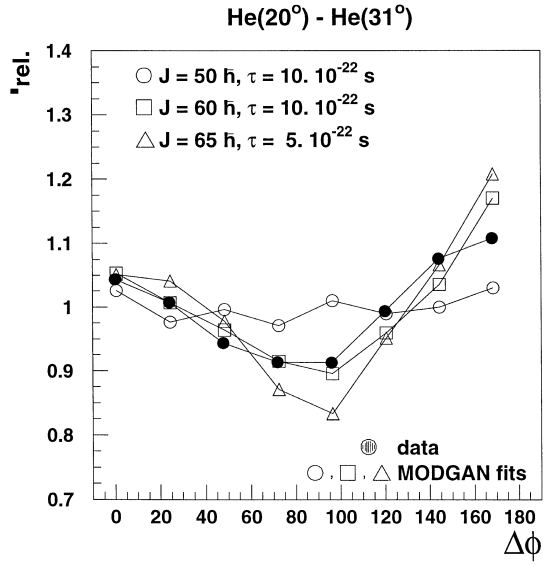

Fig. 6. Estimation of the angular momentum of the emitter using the MODGAN code simulations

4.2.3 Estimation of the angular momentum of the source and estimation of the time delay

The azimuthal correlation analysis has been performed for He-He pairs and He-Li pairs (for higher masses, statistics are poor). Figure 6 shows the distributions obtained for different values of the emitter angular momentum. The black circles are the experimental data, the open circles, squares and triangles are MODGAN calculations for three values of angular momentum. The best fit is obtained for angular momentum of $< J >= 60 \pm 10\hbar$.

Figure 7 presents the azimuthal correlations for different values of the time delay between emission of two He particles. The angular momentum is fixed from the

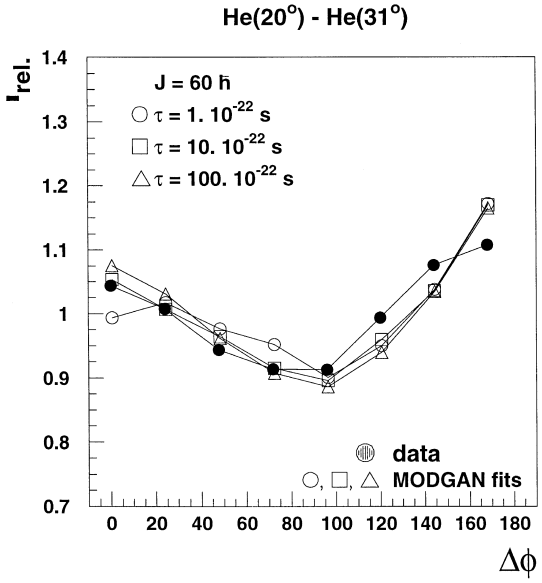

Fig. 7. Estimation of the time delay between emission of two heliums from the emitter using the MODGAN code simulations.Experimental data are the black circles, calculations are the open circles, squares and triangles

previous analysis to $< J >= 60 \pm 10\hbar$. We observe a weak lifetime effect only for the first point $\Delta\phi = 0$. Two points could explain this:

– the geometrical granularity is correct, for the charged particle multiplicity measurement, but too small to extract such tiny effect.

– as we produce reverse kinematics reaction, all the products are emitted in the forward direction, so in consequence the apparent granularity in the emitter frame is bigger than the geometrical one.

The best fits are obtained for time delay $\tau \geq 10.10^{-22}$ s (for time delay greater than this value the Coulomb effect becomes negligible). In fact, the absolute value has no particular meaning since we would like to reject the instantaneous multifragmentation scenario. As the analysis is delicate to draw definitive conclusions, we prefer the simplest scenario which is the fusion followed by a sequential decay without excluding the multifragmentation one. Moreover we have to keep in mind the small number of the $< IMF >$.

The different combinations of polar angles (20°, 31°, 47°, 67°) are shown in Fig. 8 and 9. The experimental data are represented by black circles. The curves stand for MODGAN simulation for $< J >= 60\hbar$ and $\tau = 50.10^{-22}$ s. The agreement is fairly good for seven (over ten) pairs of angles as well as for both the He-He pairs and the He-Li pairs. These azimuthal correlations strenghten our hypothesis that the selected experimental sample is mainly composed of fusion events in the sense where the analysis supposes a sequential IMF emission from an equilibrated source.

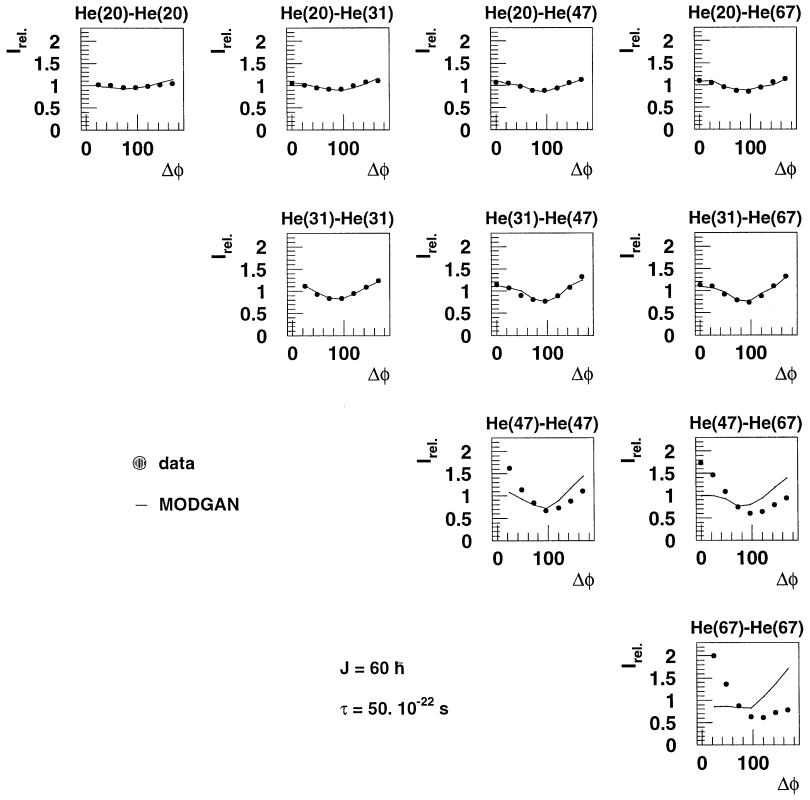

Fig. 8. He-He azimuthal correlations. Fits for the angular momentum of the emitter and for the time delay using the MODGAN simulations, for all pairs of polar angle

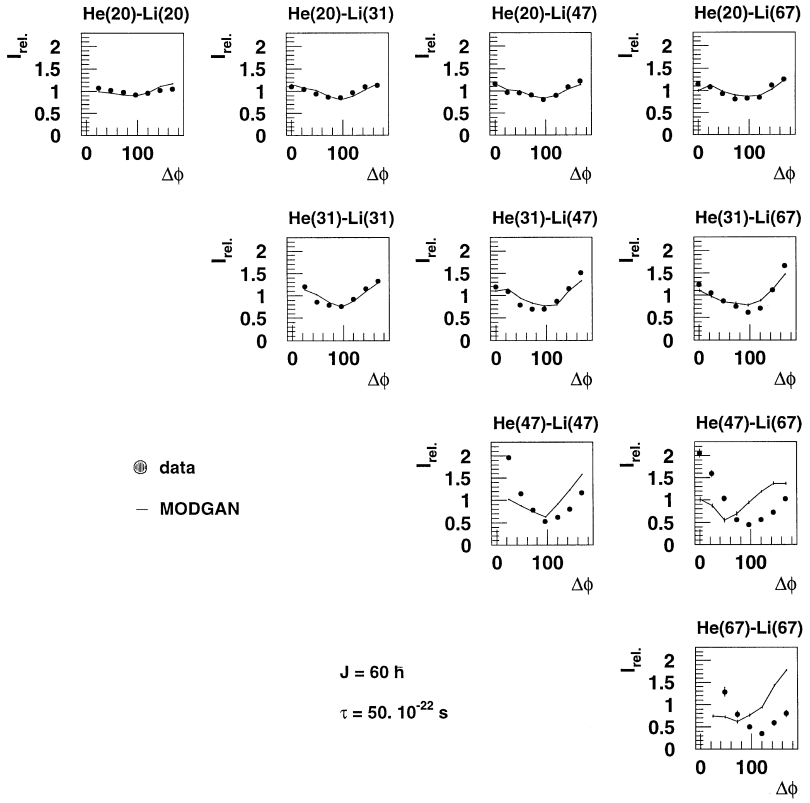

Fig. 9. He-Li azimuthal correlations. Fits for the angular momentum of the emitter and for the time delay using the MODGAN simulations, for all pairs of polar angle

5 Discussion

5.1 Azimuthal correlations

The experimental azimuthal correlation distribution shows a strong asymmetry with a maximum at small angles when polar angles are larger than $(\theta_X, \theta_Y) \geq 47°$(Figs. 8 and 9)

The DIP contribution could be an explanation but it has been checked that the construction of $\Delta\phi$ distribution for DIP events (DBS filtered and selected simulations) does not show this phenomenon. Similar effects have been observed for the $^{32}S + ^{nat.}$ Ag at 37.5 A·MeV system [22]. For this reaction the strong asymmetry is observed at forward polar angles. Preequilibrium emission which is expected to have strong dependence on the angular region is a possible interpretation of this effect. It is important to emphasize that this feature is observed only at the very backward angles for the present system which is in reverse kinematics.

5.2 Angular momentum of the emitter

Let us first show that the relatively large angular momentum obtained by the azimuthal correlation analysis is not due to a DIP contamination effect as shown in figure 10 where an effect of DIP contribution would be to enhance only the large relative angle side of the distribution. The tendancy suggested by this figure is to maximize the critical angular momentum of the fusion events.

This can be only obtained by increasing the friction coefficient in the DBS code to obtain a compound nucleus with larger angular momenta. Doing so, we observe events with a maximal angular momentum $J_{max.} = 72\hbar$, the mean value being $< J > \simeq 50\hbar$. A good agreement with the experimental data has been observed using the same variables as in Fig. 4. These comparisons confirm the validity of the MODGAN code and the azimuthal correlation method.

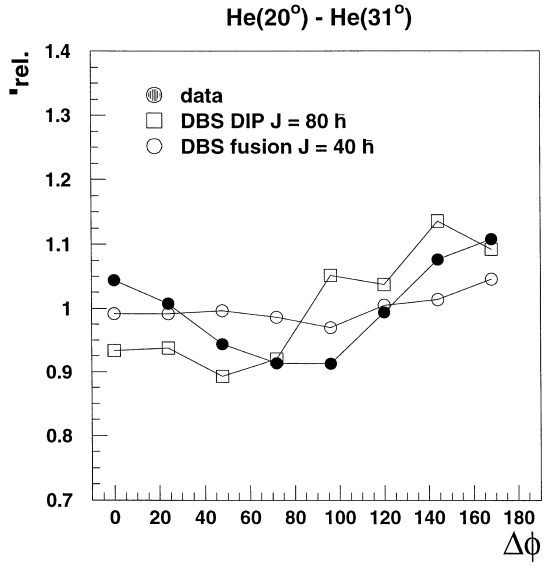

Fig. 10. He-He azimuthal correlations. The black circles are the experimental data, open circles and open squares are fits for simulated fusion and DIP events

5.3 Fusion cross section

The fusion cross section measured in our experiment is

$$\sigma^{tot}{}_{fusion} = 300 \pm 100 \text{ mbarn}$$

This cross section is obtained directly from the selected events which represent 13% of the raw data.

To correct this cross section taking into account the DIP contamination, an estimation of the experimental proportion of fusion and inelastic events has been made. The best fit based on the same variables than in Fig. 4 is obtained for 80% fusion and 20% DIP as in the DBS code prediction. After this fit the experimental cross section can be compared with the DBS code prediction. In the DBS code fusion does not occur for impact parameter larger than $b^{max}_{fusion} = 3\,fm$ and for this reaction the largest impact parameter is $b_{max} = 8.7\,fm$, so we are able to estimate the DBS fusion cross section:

$$\sigma^{tot} = \pi b^2_{max} = 2.4 \text{barn}$$
$$\sigma^{tot}{}_{fusion} = \pi(b_{fusion}/b_{max})^2 = 250 \pm 100 \text{ mbarn}$$

Finally if we increase the angular momentum of the DBS fusion events as suggested by the previous subsection, then the DBS fusion cross section rises up to 300 mbarn.

6 Summary of the source characteristics and conclusion

The deexcitation of the composite system formed by the Ni + Al reaction at 28 A.MeV laboratory energy has been studied with the 4π multidetector AMPHORA. We have observed an agreement between the experimental data and a fusion process followed mainly by a sequential decay of light particles and IMF. We have obtained these conclusions for a careful selection of events reducing as far as possible the contribution of binary events. The characteristics of the compound nucleus have been determined and then successfully compared with the MODGAN code which leads to the determination of the angular momentum of the source. All results can be interpreted in terms of sequential emission from a thermalized source with a mean angular momentum of $< J >= 60 \pm 10\hbar$. The fusion cross section measured for this sytem is $\sigma^{tot}{}_{fusion} = 300 \pm 100$ mbarn

For systems in the same mass region at larger available excitation energy the disappearance of fusion in favor of the inelastic diffusion has been observed [24]. In this reaction it seems that a large part of the excitation energy is invested in the rotational degree of freedom. Although the DBS predictions lead to a value of 5 A·MeV for the compound nucleus excitation energy, which is a value close to

the theoretical multifragmentation onset, we do not observe the multifragmentation decay as the dominant one. An analysis of the events with more than two IMF in our sample should be done for the study of this mechanism.

References

1. W. U. Schroder J. R. Huisenga Treatise on Heavy Ion Science ed. A. Bromley, volume 2, Plenum, New York (1984)
2. G. D. Westfall et al; Phys. Rev. Lett. **37** (1976) 1202
3. L. G. Moretto and G. J. Wozniak; Ann. Rev. Nucl. Part. Sci. (1993) 379, and references quoted therein
4. V. Lips et al Phys. Lett. B**338** (1994) 141
5. V. Lips et al Nucl. Phys. A**583** (1995) 585c
6. K. Hagel et al Phys. Rev. Lett. **68** (1992) 2141
7. M. Louvel et al Phys. Lett. B**320** (1994) 221
8. O. Lopez et al Phys. Lett. B**315** (1993) 34
9. N. Marie et al Phys. Lett. B**391** (1997) 15
10. D. Drain et al; Nucl. Inst. and Methods A**28** (1989) 528
11. D. Heuer; Nucl. Inst. and Methods A**324** (1993) 569
12. D. W. Stracener et al; Nucl. Inst. and Methods Phys. A**485** (1990) 485
13. D. Heuer et al; Phys. Rev. C**50** (1994) 1943
14. code DBS, A. Lleres et al; ISN Grenoble (France) (unpublished)
15. code SIR, D. Heuer et al; ISN Grenoble (France) (unpublished)
16. A. Bonasera, F. Gulminelli, J. Molitoris; Phys. Rep. vol **243** (1994) 1
17. J.R. Birkelund et al; Phys. Rep. **56** (1979) 107
18. R.J. Charity et al; Nucl. Phys. A**483** (1988) 371
19. P. Désesquelles et al; Phys. Rev. C**48** (1993) 1828
20. D.H.E. Gross; Nucl. Phys. A**553** (1993) 175c; Rep. Prog. Phys. **53** (1990) 605; Phys. Lett. B**203** (1988) 26
21. N.N. Ajitanand et al. Phys. Rev. C**34** (1996) 877; NIM A**376** (1996) 213
22. D. Benchekroun et al Zeit. fur Phys. A**356** (1997) 411
23. T. Ethvignot et al Phys. Rev. C**48** (1993) 618
24. J.L. Charvet et al; XXXV th International Winter Meeting on Nuclear Physics, Bormio (Italy) 3-8 February 1997